Annals of Nuclear Energy 212 (2025) 111013

Contents lists available at ScienceDirect

Annals of Nuclear Energy

journal homepage: www.elsevier.com/locate/anucene

Unresolved resonance parameter evaluation and uncertainty quantification of n+^{181}Ta reactions

Jesse M. Brown [a,*], Devin P. Barry [b], Amanda Lewis [b], Timothy H. Trumbull [b], Marco T. Pigni [a], Travis Greene [a], Robert C. Block [c], Alec Golas [c], Yaron Danon [c]

[a] Oak Ridge National Laboratory, 1 Bethel Valley Rd, Oak Ridge, 37831, TN, USA
[b] Naval Nuclear Laboratory, 2401 River Rd, Niskayuna, 12309, NY, USA
[c] Rensselaer Polytechnic Institute, 110 8th St., Troy, 12180, NY, USA

ARTICLE INFO

Keywords:
Tantalum
Nuclear data
Evaluation
Covariance
Unresolved resonance

ABSTRACT

Nuclear technology applications, including reactor modeling, accelerator design, and isotope production, strongly depend on evaluated nuclear data libraries and their uncertainty information for the assessment of predictive accuracy of calculated quantities. Major nuclear data libraries such as JENDL-5, JEFF-3.3, and ENDF/B-VIII.0 lack uncertainty information for n+^{181}Ta reactions. In addition to the lack of evaluated uncertainty information even in major nuclear data library releases, the most current US ENDF/B-VIII.0 evaluation of the unresolved resonance region (URR) does not extend to high enough energies to appropriately account for resonance self-shielding effects. This work addresses these shortcomings through a new evaluation of the URR, performed with the SAMMY evaluation tool, which extends the evaluation of the URR to encompass neutron energies of 2.5 keV to 100 keV. This study reports evaluated covariances and includes newly measured data in the evaluation analysis that were unavailable to previous evaluators. The new evaluation was designed to be closely coupled to the resolved resonance region evaluation to improve consistency across multiple evaluation regions. The updated cross sections in the URR have reduced capture and total cross sections, which improve agreement with differential measurements compared to ENDF/B-VIII.0, but they deviate slightly further from integral benchmarks.[1]

1. Introduction

Tantalum is an ideal material for many high-radiation environments because of its high melting temperature (Malter and Langmuir, 1939) and resistance to chemical interactions (Taylor, 1950). For these reasons, tantalum has often been used for test tubes or crucibles for handling molten salts containing actinides (Roy et al., 1996; Mullins et al., 1968; Kirkbride, 1965; El-Dasher et al., 2011). Tantalum is also used for neutron production targets, including both old (Overberg et al., 1999) and new designs (Fritz, 2022) at the Gaerttner Linear Accelerator (LINAC) Center at Rensselaer Polytechnic Institute (RPI). For neutron transport codes to accurately predict the behavior of applications that include tantalum, they must have accurate underlying evaluated nuclear data (ND). The standard procedure in the development and improvement of ND information is to store evaluated data in the Evaluated Nuclear Data File (ENDF) format (Members of the CSWEG, 2018) in one of several major evaluated libraries, including ENDF/B-VIII.0 (Brown et al., 2018), JEFF-3.3 (Plompen et al., 2020), and JENDL-5.0 (Iwamoto et al., 2019). These three libraries have discrepancies in the mean values of the tantalum neutron cross section, and none of them include covariance on those cross sections (it should be noted that the latest TENDL release does include covariance in File 33 Koning et al., 2019).

These discrepancies have been discussed thoroughly in Refs. Brown (2019), Brown et al. (2020) and Brown et al. (2023), but in general are due to differences in evaluator decisions on what energy region the unresolved resonance region (URR) should be used, and how to represent the cross sections and self-shielding in those regions. ENDF/B-VIII.0 employed the URR in the energy region of 330 eV to 5 keV, causing serious inaccuracies due to resonance self-shielding above 5

* Corresponding author.
E-mail address: brownjm@ornl.gov (J.M. Brown).

[1] This manuscript has been authored by UT-Battelle, LLC under contract DE-AC05-00OR22725 with the US Department of Energy (DOE). The US government retains and the publisher, by accepting the article for publication, acknowledges that the US government retains a nonexclusive, paid-up, irrevocable, worldwide license to publish or reproduce the published form of this manuscript, or allow others to do so, for US government purposes. DOE will provide public access to these results of federally sponsored research in accordance with the DOE Public Access Plan (http://energy.gov/downloads/doe-public-access-plan).

https://doi.org/10.1016/j.anucene.2024.111013
Received 3 July 2024; Received in revised form 10 October 2024; Accepted 21 October 2024
Available online 13 November 2024

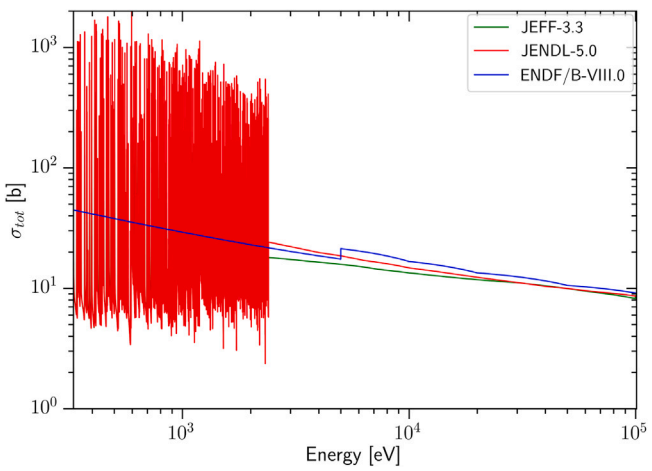

Fig. 1. ENDF/B-VIII.0, JEFF-3.3, and JENDL-5.0 have several differences in the URR, including how to calculate the infinitely dilute cross section, where the URR region should reside, and how to represent cross section fluctuations.

keV. JEFF-3.3 employs the URR from 2.4 keV up to 100 keV which covers all the energies where self-shielding is significant and dictates that average resonance parameters should be used to calculate the infinitely dilute cross section. JENDL-5 is quite similar to the JEFF-3.3 evaluation with URR from 2.4 to 100 keV, but provides explicit pointwise cross section values for the infinitely dilute cross section in the URR (as recommended in Ref. Leal et al. (2011)). The total cross section in the URR of the three libraries included in this study are shown in Fig. 1.

Recent neutron capture and transmission measurements at RPI by Brown et al. (2023) show that ENDF/B-VIII.0 should be re-evaluated based on its poor performance modeling thick-sample neutron transmission, in addition to the lack of covariance data in all major ND libraries. Those new measurements, in addition to several legacy measurements, were used in this work to update the evaluated parameters in the URR. These new evaluated data were then used to model both differential and integral validation experiments in radiation transport codes to compare the performance of the new evaluated data to existing ND libraries. The new evaluated data were included in the recent release of ENDF/B-VIII.1.[2]

2. Measurements

Experimental data play two fundamental roles in nuclear data evaluation: (1) to inform semi-empirical models through model-parameter optimization in the evaluation process, and (2) to assess that the semi-empirical models and fitted parameters can be used to predict radiation transport in the validation process. It is important to note that the datasets used to inform the semi-empirical models cannot be used for validation of those same models because the models are biased to the data by which they were informed. In this work, we chose to evaluate mostly high-energy-resolution and thin-sample experiments, and to use thick-sample differential measurements and criticality measurements for validation.

There were three parallel evaluations of tantalum, including this one, in the following energy regions:

1. **0–2.5** keV in the resolved resonance region (RRR) by Barry et al. (2024),
2. **2.5–100** keV in the URR for the present work, and
3. **0.1–20** MeV in the fast region by Herman and Kawano (2024)

Several experimental datasets are available to inform these three parallel evaluation efforts. The datasets that directly informed the URR evaluation presented for this work are given explicitly. Some of these datasets overlap multiple regions of the RRR, URR, and fast regions, and they were therefore also used in the parallel evaluations by Herman et al. and Barry et al. The full set of evaluation datasets used in the RRR is given in Ref. Barry et al. (2024).

Data used in multiple evaluation regions include capture yield measurements by McDermott et al. (2017) and McDermott (2016), high-resolution transmission by Harvey et al. (1988), new transmission and capture yield measurements by Brown et al. (2023, 2020), and total cross section by Poenitz et al. (1981). Many other low-resolution total (σ_t), elastic (σ_n), and capture (σ_γ) cross section measurements (Wisshak et al., 1990, 2004; Brzosko et al., 1969; Bokhovko et al., 1991; Kononov et al., 1977; Yamamuro et al., 1980; Zo et al., 1985; Otuka et al., 2014) performed in the URR in the past few decades were included in this evaluation. Except those of McDermott et al. (2017) and Brown et al. (2023), measurements used in this evaluation were chosen based on their availability in the EXFOR database (Otuka et al., 2014) and whether they included reliable uncertainty information and sufficient documentation.

Several EXFOR datasets required re-normalizations. The two Wisshak datasets (Wisshak et al., 1990, 2004) were published as ratios to ^{197}Au(n,γ), so they were converted to capture cross section by pointwise normalization to the standard capture cross sections for gold published by Carlson et al. in 2018 (Carlson et al., 2018) (hereinafter referred to as the *2018 standard*). The Kononov dataset (Kononov et al., 1977) was originally normalized to gold at 30 keV, so this was re-normalized to the 2018 standard at 30 keV. The McDermott dataset was originally normalized to the 2009 cross section standard for ^{10}B$(n,\alpha_1\gamma)$ by Carlson et al. (2009), but because the 2009 and 2018 standards are less than 0.1% different at 4 eV, the data were left unchanged. The 2018 standard for ^{197}Au(n,γ) between 2.5 and 200 keV has an uncertainty varying between 1.8 and 2.6%, and ^{10}B$(n,\alpha_1\gamma)$ at approximately 4 eV has an uncertainty of 0.9%. These uncertainties were incorporated into the normalization uncertainties for experimental cross sections as part of the Bayesian prior for the evaluation.

Experimental data used to validate the posterior model parameters from the Bayesian analysis are thick-sample transmission from Brown et al. (2020), thick-sample transmission and self-indication from Byoun (1973a,b), and criticality benchmark data from the International Criticality Safety Benchmark Project (ICSBEP) (International, 2022) by Percher et al. (2023). Data from Byoun et al. exist in EXFOR, but they are now updated as they were recently retrieved from Byoun's 1973 thesis so as to include more information than was previously available in EXFOR. The datasets from Byoun and Brown were ideal for validation as opposed to evaluation because of the thickness of samples that were used. These thick-sample measurements require well-characterized resonance evaluations (RRR and URR) to properly predict resonance self-shielding.

3. Evaluation methodology

In this work, the tantalum URR analysis ranges from neutron incident energies in the 2.5–100 keV range. Evaluation in the URR was performed with the Bayesian evaluation code SAMMY (Larson, 2008). The SAMMY code includes multi-level Breit–Wigner (MLBW) and Reich–Moore (RM) R-matrix (Lane and Thomas, 1958) cross section models in the RRR and the Hauser–Feshbach (HF) cross section model in the URR by incorporation of Fröhner's FITACS code. For this evaluation, the SAMMY code solved Bayes' equation using the generalized least squares (GLS) method.

[2] Due to an unfortunate clerical error, the URR covariances for ^{181}Ta in the final ENDF/B-VIII.1 release were unintentionally overwritten in the process of file assembly with higher values that are incorrect but more conservative. It is anticipated that future versions of the US ENDF/B library and/or errata will use the values in this paper.

SAMMY requires several average resonance parameters to calculate the average HF reaction cross sections. Those related to the statistical analysis of resonances given for each orbital angular momentum l are the neutron strength functions, S_l, distant-level parameters, R_l^∞, average radiation widths, $\langle \Gamma_{\gamma,l} \rangle$, s-wave neutron interaction radius, $a_{l=0}$, and average s-wave level spacing, $D_{l=0}$. In addition, SAMMY also requires parameters related to nuclear structure, such as the pairing, PE, and neutron binding, BE, energies together with the excited states of the target nucleus.

To achieve consistency between the RRR and URR, an automated process was implemented to incorporate the evaluated parameters from Barry et al. (2024). The posterior resonance parameters from the RRR evaluation were used to calculate average resonance parameters for the HF calculations in the URR. This feed-forward automation process provides full freedom to both the RRR and URR evaluator on decisions for cross section models and data, but it also enforces consistency of the RRR posterior resonance parameters and the prior average resonance parameters in the URR.

To avoid the possibility of "missing" nuclear levels affecting the average resonance parameter calculations, the resonance parameters used for HF input were taken from resonances below 300 eV. D_0 is the mean distance between resonances energies (only s-waves observed), $\langle \Gamma_{\gamma,l} \rangle$ is a simple average taken over the fitted radiation widths from the RRR, and the distant-level parameter is taken as follows:

$$R_0^\infty = 1 - \frac{R'}{a_0}, \tag{1}$$

where R' is an effective radius from Barry et al. The neutron strength function for s-waves, S_l, is calculated for the URR by the formula in Mughabghab (2006), where

$$S_l = \frac{1}{(2l+1)\Delta E} \sum_\lambda g_\lambda \Gamma_{\lambda,n}^l, \tag{2}$$

$$\Gamma_{\lambda,n}^l = \sqrt{\frac{1\text{eV}}{E_0}} \frac{\Gamma_{\lambda,n}}{V_l}, \tag{3}$$

and,

$$V_l = \frac{P_l}{\rho}. \tag{4}$$

Here, $\Gamma_{\lambda,n}$ is the observed neutron width, P_l is the hard sphere penetrability, g_λ is the spin statistical factor, $\Delta E = 300$ eV, and $\rho = k_c a_c$: the wave number multiplied by the channel radius. The SAMMY code uses the s-wave level density ($1/D_0$) at the binding energy (i.e., zero kinetic energy of the neutron) and the Gilbert–Cameron composite level density formula (Gilbert and Cameron, 1965) to compute level density as a function of energy and compound nuclear spin.

To model neutron transport for n+^{181}Ta reactions, resonance self-shielding effects must be properly modeled over the URR range. Because SAMMY HF cross section models do not yet account for self-shielding (SS) or multiple-scattering (MS), an external code, SESH (Fröhner, 1968; Fröhner and Brown, 2021), was used to correct the experimental cross sections. The correction was calculated based on the average resonance parameters and a simple description of the sample geometry. The correction brings the experimental data to the "true" (or infinitely dilute) cross section, which can be directly compared to theoretical cross sections calculated by SAMMY. This correction can be significant at lower URR energies: the largest corrections were made to the 6 mm transmission and 2 mm capture yield measurements by Brown et al. as shown in Fig. 2. SESH corrections were found to be reliable while they were less than 50%.

SESH produces correction factors for experimental transmission data, C_T, and experimental capture yield, C_Y, based on the same average resonance parameters as those of SAMMY plus a simple description of sample geometry. The corrections were applied directly to the transmission, T_{exp}, and capture yield, Y_{exp}, where

$$\sigma_{t,exp} = \frac{1}{n} \ln\left(\frac{\langle T_{exp} \rangle}{C_T}\right), \qquad C_T = \frac{\langle e^{-n\sigma_t} \rangle}{e^{-n\langle \sigma_t \rangle}}, \tag{5}$$

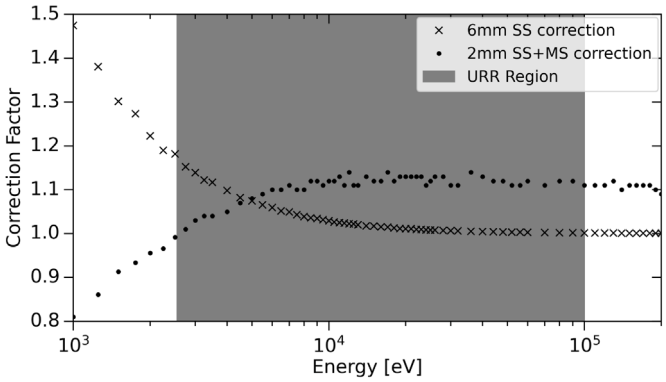

Fig. 2. The energy-dependent correction factor as calculated by SESH for data from Brown et al. in the energy region of the present evaluation. The SS correction factor was observed to increase quickly for 6 mm transmission as neutron energy decreased. SS and MS corrections for the 2 mm capture measurement were up to 10%. It is noteworthy that the combined contribution from SS and MS corrections for the capture samples could increase or decrease the experimental cross section.

and

$$\sigma_{\gamma,exp} = \frac{\langle Y_{exp} \rangle}{nC_Y}, \qquad C_Y = \frac{\langle Y_{sim} \rangle}{n\langle \sigma_\gamma \epsilon \rangle}, \tag{6}$$

as defined in Ref. Fröhner (1968). In this framework, n is the sample thickness in at./b, $\langle \sigma_\gamma \epsilon \rangle$ is the "average effective cross section", and Y_{sim} is a Monte Carlo simulated yield. The experimental capture cross section formula shown above is the "thin-sample" approximation, which comes from the Taylor series expansion of the exponential term

$$\begin{aligned} \sigma_\gamma &= Y\sigma_t (1 - e^{-n\sigma_t})^{-1} \\ &= Y\sigma_t \left(1 - 1 + n\sigma_t - \frac{(n\sigma_t)^2}{2!} + \cdots\right)^{-1} \\ &\approx \frac{Y}{n}, \end{aligned} \tag{7}$$

where $n\sigma_t \ll 1$. SESH requires very similar input to that required by the SAMMY/FITACS code for average resonance parameters, but it also requires geometric information about the sample.

The equations above show that SESH corrections require knowledge of the final average resonance parameters. This creates a circular problem, as SAMMY requires SESH corrected data prior to calculating the final posterior parameters. For this reason, the following loop was executed:

1. The prior average resonance parameters calculated from the RRR are given to SESH to correct the experimental data.
2. The prior average resonance parameters calculated from the RRR and SESH-corrected data are given to SAMMY to calculate posterior evaluated parameters.
3. The posterior parameters are given to SESH to calculate corrections.
4. Repeat 2–3 until the parameters used in SESH have converged with the posterior parameters calculated by SAMMY.

The prior (as calculated from the RRR) and final posterior average resonance parameters are listed in Table 1.

Because only s-waves were apparent in the RRR analysis, the prior $S_{l=1,2}$ values were taken from Mughabghab (2018). We also note here that the channel radius $a_c = 7.86 \pm 0.24$ fm was kept the same as the RRR in the work by Barry et al. (2024) and that in the RRR fitting $a_c = R'$ (as in R_c^∞ is assumed to be zero). This results in an s-wave channel radius that is consistent from the thermal energy region to 100 keV and consistent with the calculated penetrabilities for all resonance parameters. The p- and d-wave distant-level parameters, R_1^∞ and R_2^∞, were kept constant (and equal to s-wave) to conform to current ENDF formats, which allow only a single channel radius for all channels. The binding

Table 1
URR average parameters for ^{181}Ta. Some parameters were not varied (NV) during the analysis. S_l are given in units of 10^{-4}; D_0 and $\langle\Gamma_{\gamma,l}\rangle$ are in units of eV.

Par.	Prior	Posterior
D_0	4.1	4.1 (NV)
S_0	1.78 ± 0.57	1.69 ± 0.04
S_1	0.50 ± 0.20	0.76 ± 0.07
S_2	2.30 ± 0.30	1.63 ± 0.17
R_0^∞	0.0 ± 0.1	0.017 ± 0.011
R_1^∞	0.017	0.017 (NV)
R_2^∞	0.017	0.017 (NV)
$\langle\Gamma_{\gamma,0}\rangle$	0.0678 ± 0.012	0.0646 ± 0.0025
$\langle\Gamma_{\gamma,1}\rangle$	0.0678 ± 0.012	0.0449 ± 0.0023
$\langle\Gamma_{\gamma,2}\rangle$	0.0678 ± 0.012	0.0646 ± 0.0025

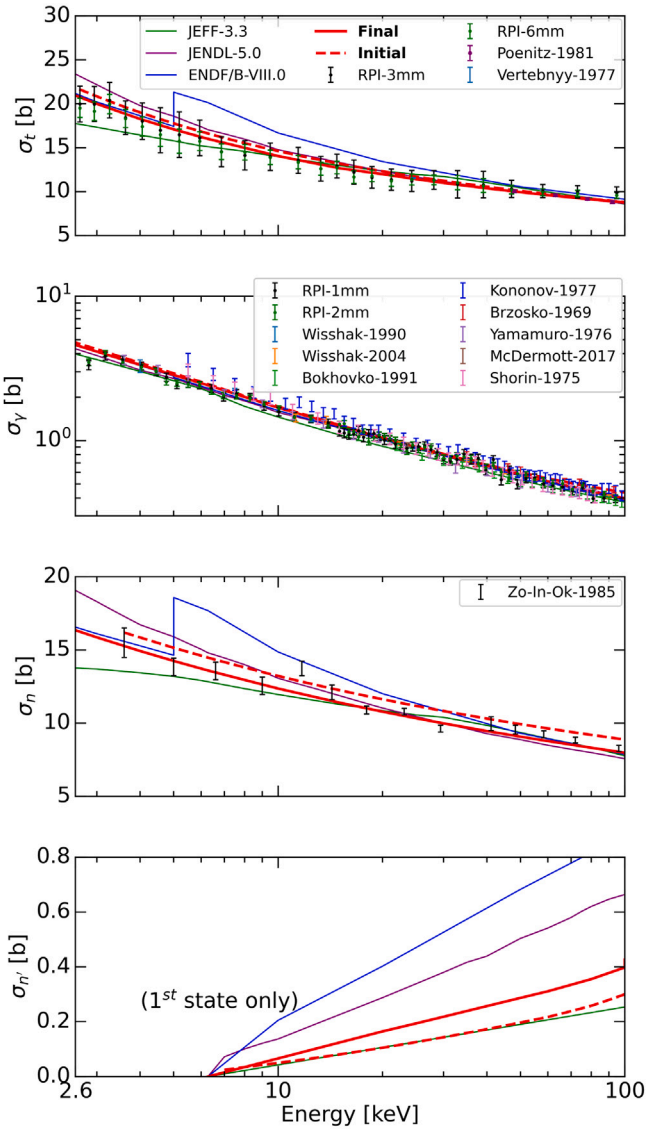

Fig. 3. Initial and final evaluated cross sections for each reaction are represented by the dashed and solid bold red lines, respectively. The final evaluated cross sections closely followed low-uncertainty data from Poenitz et al. and Wisshak et al. Note that subscripts t, γ, n, n' represent the total, capture, elastic, and inelastic reactions, respectively. ENDF/B-VIII.0, JEFF-3.3, and JENDL-5.0 are plotted for each reaction with consistent color.

energy, BE, was set to 6.06296±0.00016 MeV according to Mughabghab (2018), and the pairing energy for neutrons, PE, was set to zero. The ground-state spin of ^{181}Ta is $7/2^+$, the first excited state is $9/2^-$ at 6.237

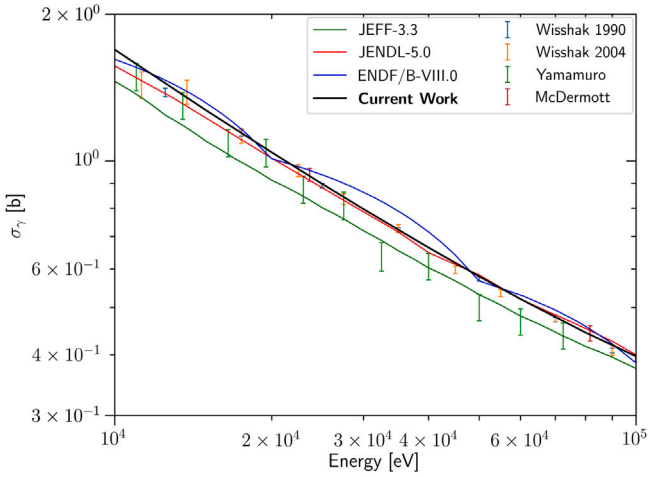

Fig. 4. The new evaluated capture cross section in the URR has changed by a small amount, but agrees better with reported experimental data than ENDF/B-VIII.0.

keV, and second excited state is $9/2^+$ at 136.262 keV, as reported in the ENSDF library by Wu (2005). Because the 6.237 keV line is very difficult to measure[3] in neutron inelastic scattering cross section ($\sigma_{n'}$) experiments, no cross section data have been reported for that reaction. In terms of the evaluation, this means that the inelastic cross section below approximately 136 keV is largely unconstrained except by the summation $\sigma_t = \sigma_n + \sigma_\gamma + \sigma_{n'}$, where measurements are available for all cross sections except inelastic. Normalization factors for each dataset were included in the evaluation, and the prior and posterior values are given in Appendix. The final evaluated cross sections as modeled by SAMMY are compared to the fitted data in Fig. 3.

A magnified comparison of the final evaluated capture cross section to the other nuclear data libraries is shown in Fig. 4. The current evaluated capture cross section is on average ≈1.8% less than ENDF/B-VIII.0 in the energy region from 2.6–100 keV. This small change agrees better with the reported experimental data, especially the two datasets by Wisshak between 20–100 keV. It also becomes more obvious that the change is not only a simple change in cross section magnitude, but also the way in which the cross section is processed from the ENDF file itself. In the ENDF/B-VIII.0 file, the evaluator-provided grid is not coarse enough to use linear interpolation as the evaluator prescribed, resulting in the interpolated cross section missing the experimental data.

The covariance on the posterior parameters given in Table 1 was used to calculate pointwise covariance for cross sections in order to best represent the evaluation in the ENDF format. This pointwise covariance can then be used by ENDF users for transport codes. For the plots in this work, the evaluated data processing code AMPX (Wieselquist and Lefebvre, 2021) was used to produce 252-group covariances for the groupwise cross section (group energy structure is listed in Ref. Wieselquist and Lefebvre (2021)). The resulting correlation matrices for each reaction and cross-reaction are plotted in Fig. 5. It is worth noting that when propagating these covariances forward to an application response, the resulting uncertainty on that response could increase or decrease depending on whether the product of the application sensitivity coefficient and covariance is positive or negative, respectively. For instance, the energy-dependent covariance of capture with itself was positive for much of the matrix. A response such as reactor multiplication factor k_{eff} would have a negative sensitivity to capture cross section; therefore, positive correlations would increase uncertainty on k_{eff}. The ENDF/B-VIII.0, JEFF-3.3, and JENDL-5.0 evaluations of ^{181}Ta did not report any evaluated covariance.

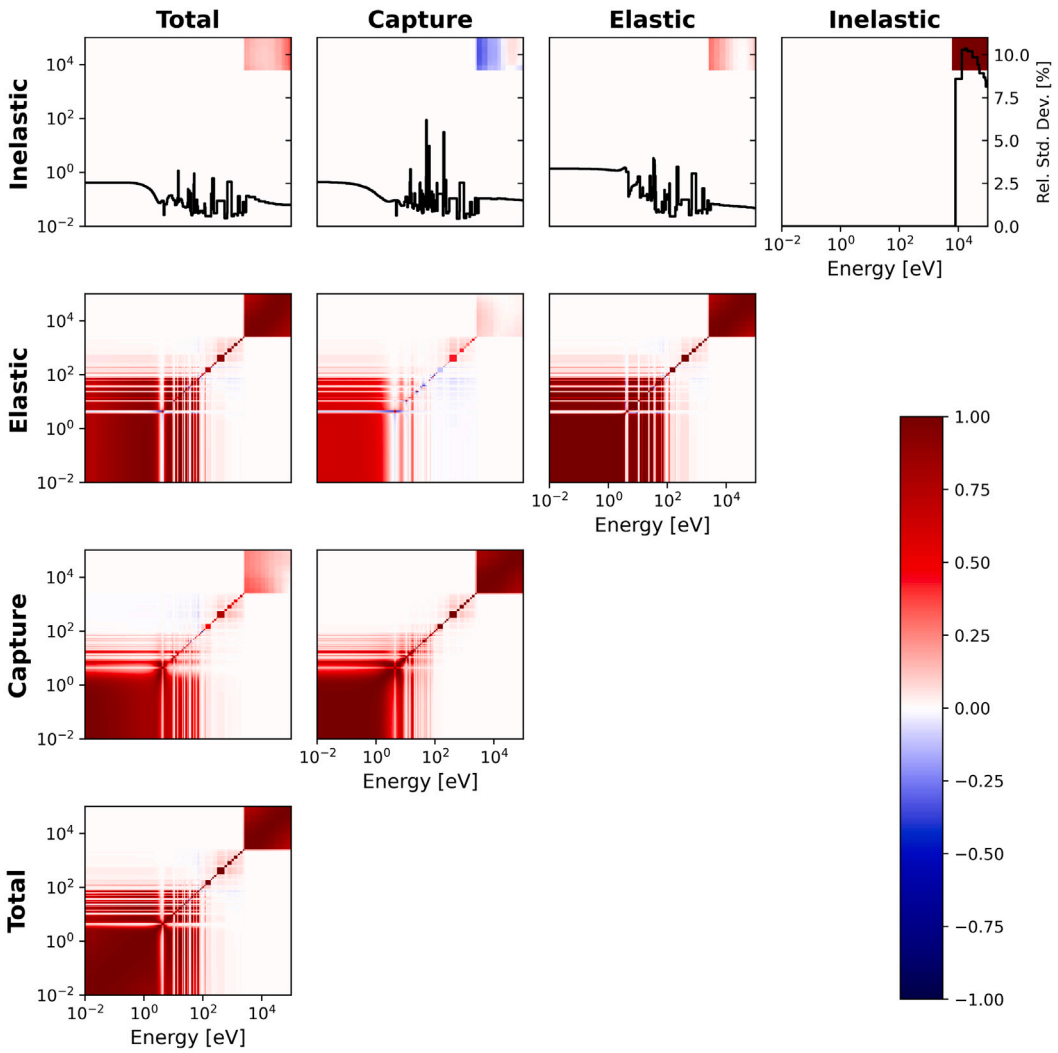

Fig. 5. The posterior correlation matrix propagated from the Bayesian analysis calculated for a 252-group cross section. In the top row representing the correlation of the inelastic reaction to all other available reactions, small correlations can be seen only in the range from 6.7 keV to 100 keV, where the reaction is energetically possible. Also in the top row a second y-axis represents relative standard deviation, with the values plotted as a function of energy in black.

4. Validation and implications for criticality

To validate the evaluated cross sections, a combination of integral and differential testing was performed, providing a more stringent test of whether the cross sections are predictive of real-world measurements. In this work, three experiment types were compared to evaluated cross sections: thick-sample transmission measurements, thick-sample self-indication measurements, and a criticality benchmark. One set of thick-sample transmission and self-indication measurements was performed by Byoun (1973a), another thick-sample transmission measurement was by Brown et al. (2020), and the Thermal/Epithermal Experiment (TEX) criticality benchmarks using Ta were performed by Percher et al. (2023).

4.1. Differential measurement validation

Thick-sample transmission measurements have proven to be useful tools to demonstrate the validity of evaluated data in the URR (Brown et al., 2020). Thick-sample transmission comparisons can expose unrealistic values for parameters such as channel radius a_c, s-wave distant-level parameter R_0^∞, and level spacing D_0. This motivated further testing with a greater range of measurements, such as those by Byoun at RPI (Byoun, 1973b,a). Byoun et al. measured transmission and self-indication ratios for multiple sample temperatures and thicknesses; this analysis includes the room temperature (~300 K) measurements for multiple thicknesses. These measurements were modeled in MCNP 6.2 (Werner et al., 2017) using the ENDF/B-VIII.0 library for all nuclides except for ^{181}Ta, which used custom ACE files from the "Present Work", as labeled in the figures that follow, and the other evaluations. The custom ACE files were produced by processing the JEFF-3.3, JENDL-5.0, and new ^{181}Ta ENDF file with updated RRR (by Barry et al. (2023)) and URR using NJOY2016 (MacFarlane et al., 2017). The resulting transmission comparison to Byoun et al. is shown in Fig. 6.

Compared to ENDF/B-VIII.0, the new evaluation in the URR brings predicted neutron transmission closer to the true measured transmission as reported by Byoun et al. The improved values for distant-level parameter R_0^∞ and s-wave strength function S_0 likely had the greatest impact on the improvements for modeled transmission. The new evaluated data from JENDL-5.0 performs the best in this energy region compared to the Byoun transmission data. The χ^2 values for evaluations compared to Byoun are given in Table 2.

[3] This line is difficult to measure because it is very soft. The low energy of the photon means it is very unlikely to escape the sample of interest, interact with the detector volume, or overcome background photon signal.

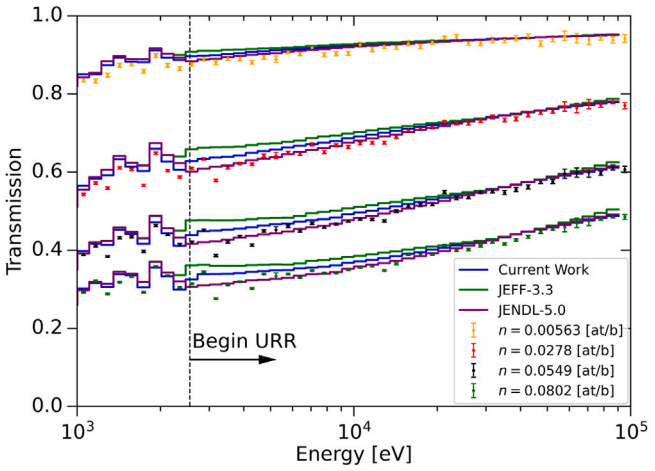

Fig. 6. Transmission measurements by Byoun (1973b) of varying sample thickness at ~300 K compared to MCNP 6.2 modeled transmission for the new evaluated data, JEFF-3.3, and JENDL-5.0 (all materials other than ^{181}Ta use ENDF/B-VIII.0 cross sections). The results with ENDF/B-VIII.0 cross sections for ^{181}Ta were not plotted to prevent the figure from becoming illegible. Monte Carlo error for transmission is less than 1%.

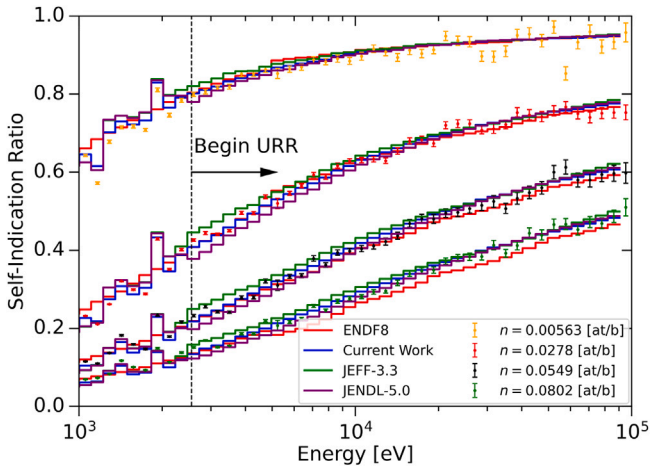

Fig. 7. Self-indication ratio measurements by Byoun (1973b) of varying sample thickness at ~300 K compared to MCNP 6.2 modeled self-indication ratio for the new evaluated data, JENDL-5.0, and JEFF-3.3 (all materials other than ^{181}Ta use ENDF/B-VIII.0 cross sections). Monte Carlo error for self-indication is less than 1%.

Table 2
All evaluations in the study were compared to the Byoun data in the URR energy region using a χ^2 metric. The χ^2 value for each evaluation is given in the table below.

Type	n [at/b]	ENDF/B-VIII.0	JEFF-3.3	JENDL-5.0	Current
T	0.00563	0.021	0.049	**0.013**	0.026
T	0.0278	0.356	0.241	**0.029**	0.083
T	0.0549	1.112	0.330	**0.043**	0.118
T	0.0802	2.030	0.424	**0.066**	0.164
SIR	0.00563	0.042	0.052	0.037	**0.034**
SIR	0.0278	0.032	0.059	0.103	**0.027**
SIR	0.0549	0.031	0.077	0.057	**0.028**
SIR	0.0802	0.097	0.060	0.066	**0.029**

Self-indication ratio (SIR) measurements require two samples: a transmission sample and a capture sample. Neutrons will first pass through the transmission sample then strike the capture sample. The ratio of capture yield for a sample in and out of the beam is then taken as Byoun (1973a)

$$SIR = \frac{\int Y_\gamma(E,T_2,n_2)e^{-n_1\sigma_t(E,T_1)}dE}{\int Y_\gamma(E,T_2,n_2)dE}, \tag{8}$$

where $Y_\gamma(E,T_2,n_2)$ (as defined by Byoun) is the capture yield for a temperature, T_2, and areal number density, n_2. Subscripts in Eq. (8) denote either sample 1 or 2 in the experiment. As indicated in Eq. (8), the SIR tests both the transmission probability and the neutron capture probability. The self-indication ratio measurements by Byoun et al. provide a test for the evaluated average capture widths $\langle\Gamma_{\gamma,l}\rangle$ in combination with the other parameters. Plots of the new evaluation compared to JEFF-3.3, JENDL-5.0, and ENDF/B-VIII.0 are shown in Fig. 7. The measured data are close to the evaluations in the URR (energies > 2.554 keV), but the χ^2 values of the new evaluation are slightly better than any other library. The difference between the two libraries is most evident at lower energies, where resonance self-shielding has the greatest impact.

The modeled transmission using the new evaluation was also compared to the transmission by Brown et al. (2020), which used a 12 mm sample to exaggerate the self-shielding effect. This experiment also included a transmission measurement of a thick ^{238}U sample to validate the experimental analysis. The ^{238}U and ^{181}Ta transmissions were grouped heavily and compared to MCNP 6.2 simulations of the experiments using ENDF/B-VIII.0 for all materials except for ^{181}Ta cross sections, which were swapped for various evaluations, as shown in Fig. 8.

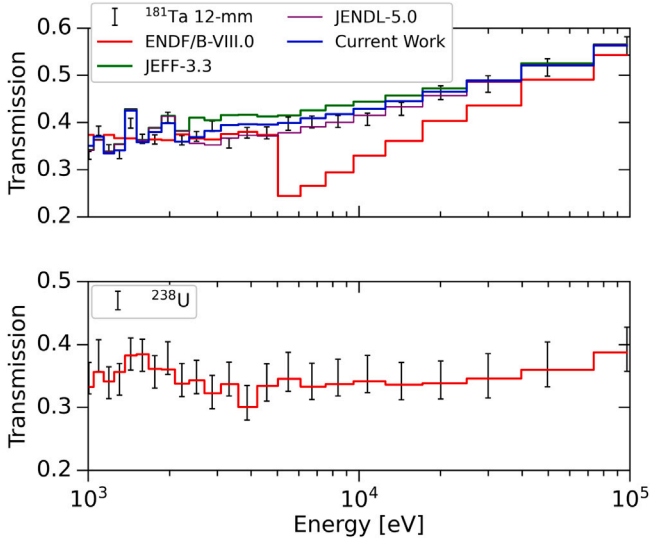

Fig. 8. Transmission measurements by Brown et al. of a 12 mm Ta sample compared to a MCNP 6.2 model of transmission using the new evaluated data, ENDF/B-VIII.0 (red), JEFF 3.3 (green), and JENDL 5.0 (purple). We note that the reference sample of ^{238}U is modeled well with the ENDF/B-VIII.0 evaluation cross sections. Note that all MCNP models used ENDF/B-VIII.0 for all materials but ^{181}Ta, which was swapped for various other evaluations.

4.2. Criticality validation

Validation of the proposed changes to the ^{181}Ta URR was also accomplished using the plutonium TEX (TEX-Pu) with a tantalum diluent, adopted as PU-MET-MIXED-003 (PMM003) in the latest edition of the ICSBEP Handbook (Percher et al., 2023), analyzed using MCNP 6.2 (Werner et al., 2017) and SCALE 6.3 (Wieselquist and Lefebvre, 2021). PMM003 consists of five cases with neutron energy spectra ranging from fast to thermal, based on the amount of moderator included in the benchmark, making this benchmark ideal for validating changes in the resolved resonance, unresolved resonance, and fast energy ranges. The sensitivity profiles of the five cases described are plotted for neutron elastic (σ_n) and neutron capture (σ_γ) cross sections in Fig. 9.

The base case analysis used ENDF/B-VIII.0 nuclear data (Brown et al., 2018) for all isotopes in the model. The ACE files were taken

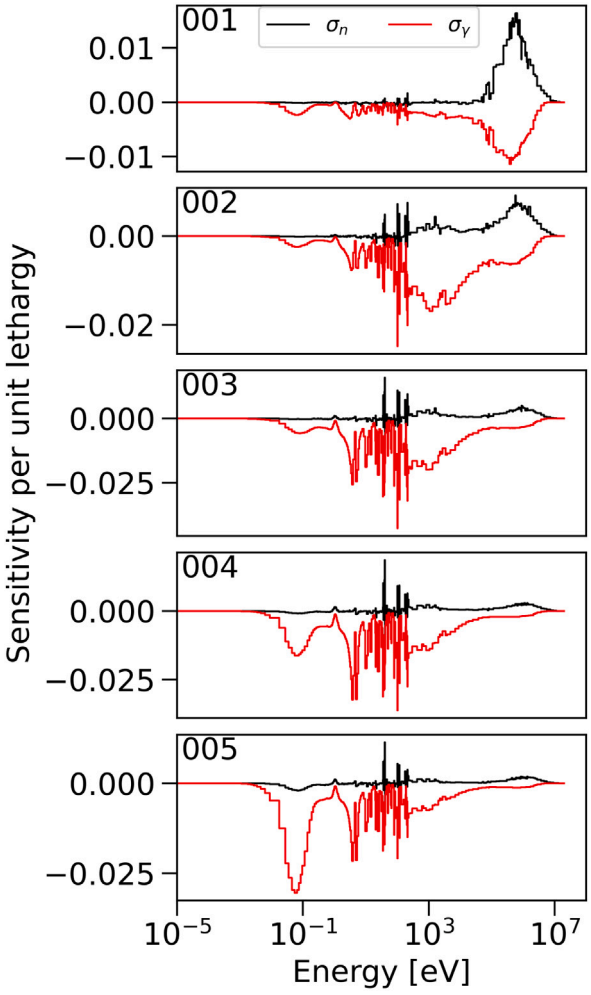

Fig. 9. Sensitivity to k_{eff} for benchmark PMM003 for cases 1–5. Increases in the elastic cross section (black) largely increase reactivity in the benchmark, while increased capture decreases reactivity. Case 002 has the largest sensitivity to the cross sections in the URR.

from the Lib80x library (Conlin et al., 2018). Additional results were generated by swapping in different nuclear data sources for ^{181}Ta only, while keeping the remaining nuclear data from ENDF/B-VIII.0. ^{181}Ta ACE files for JEFF-3.3 (Plompen et al., 2020), JENDL-5.0 (Iwamoto et al., 2019), and the present work were generated using NJOY2016.70 (MacFarlane et al., 2017). Cross sections were Doppler broadened to 293.6 K using BROADR, with probability tables generated for the URR using PURR. Probability tables were constructed using 20 probability bins and 32 resonance "ladders". Note that the "Present Work" referred to here builds upon and includes updates to the ENDF/B-VIII.0 RRR, as detailed by Barry et al. (2024), and the URR evaluation described in this work (but no fast energy region changes).

It should be noted that comparisons of the transmission and self-shielding validation above with the single nuclide "swaps" were fair comparisons of overall behavior between neutron libraries, since only ^{181}Ta is really needed to model them. Comparisons of *benchmarks* swapping only a single nuclide, however, cannot necessarily make a statement about the quality of one library (e.g. JEFF-3.3 and JENDL-5.0) over the other. Evaluations in a nuclear data libraries are almost always correlated and therefore must be used together in order to get the behavior intended by the library curators. The swapping of evaluations in this publication is intended to show the impact of changing only the ^{181}Ta evaluation, rather than making a statement on the overall quality of an entire library for a given benchmark.

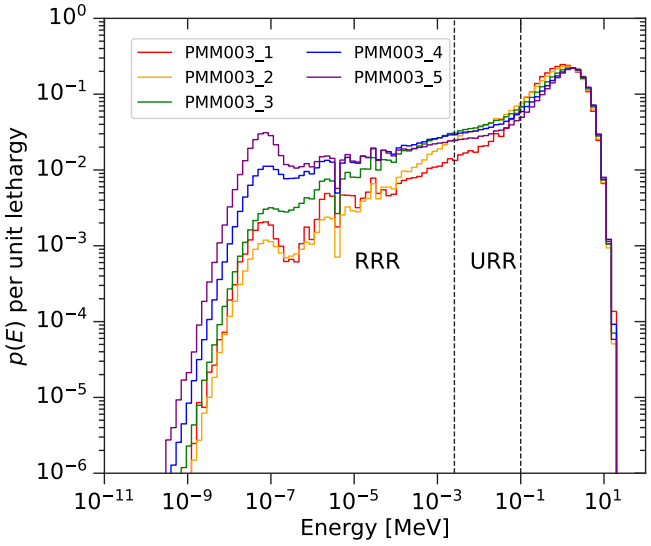

Fig. 10. Normalized neutron flux spectra for PMM003 in the tantalum regions, Cases 1–5. Note that cases 2–4 show higher fluxes in the URR proposed in this work.

Table 3
Effect of using URR probability tables for the base case, ENDF/B-VIII.0, and for the present work (including RRR changes by Barry et al.). Note the substantial impact to both the base case and this work when the ^{181}Ta URR probability tables are used, indicating sensitivity to the URR. Uncertainties on k_{calc} were from a 95% confidence interval.

ENDF/B-VIII.0	With p-table		W/o p-table		Difference	
	k_{calc}	Unc.	k_{calc}	Unc.	Δk_{calc}	Unc.
Case						
1	1.00956	0.00022	1.00402	0.00020	**0.00554**	0.00030
2	1.00771	0.00022	0.97990	0.00020	**0.02781**	0.00030
3	1.00720	0.00022	0.97842	0.00022	**0.02878**	0.00031
4	1.00272	0.00024	0.98428	0.00024	**0.01844**	0.00034
5	0.99952	0.00024	0.99005	0.00024	**0.00947**	0.00034
Present work						
	k_{calc}	Unc.	k_{calc}	Unc.	Δk_{calc}	Unc.
Case						
1	1.01032	0.00022	1.00884	0.00022	**0.00148**	0.00030
2	1.00709	0.00022	1.00380	0.00022	**0.00329**	0.00030
3	1.00471	0.00024	1.00254	0.00024	**0.00225**	0.00030
4	1.00141	0.00024	1.00022	0.00024	**0.00119**	0.00030
5	0.99955	0.00022	0.99875	0.00024	**0.00080**	0.00030

It is expected that the PMM003 benchmark model will exhibit sensitivity to changes in the ^{181}Ta URR because of the range of neutron energy spectra covered by the 5 cases, as shown in Fig. 10. The sensitivity will be compounded by the fact that the ENDF/B-VIII.0 ^{181}Ta evaluation itself contains RRR parameters up to only 330 eV, with a URR extending up to only 5 keV. Given that this work builds on an extension of the RRR to 2.554 keV (Barry et al., 2024), the sensitivity to the ^{181}Ta URR is expected to be reduced for cases that are highly moderated. We also note, however, that because the URR in this work was extended to 100 keV, sensitivity may still increase for cases with harder neutron spectra.

A predictor of how sensitive a model will be to resonance self-shielding in a particular isotope's URR is the response to running the calculation with and without using probability tables for that isotope. As seen in Table 3 under the heading "ENDF/B-VIII.0", there is an enormous reactivity change for the base ENDF/B-VIII.0 case, and a reduced (but substantial) reactivity change for this work is shown in Table 3 under heading "Present Work". Therefore, it is expected that the models will be sensitive to changes in the URR, with cases 2 and 3 being the most sensitive.

Table 4
Benchmark and calculated results for PMM003 using nuclear data from ENDF/B-VIII.0 for all other nuclides and ^{181}Ta evaluations from JENDL-5.0, JEFF-3.3, and the present work.

Case	Benchmark		ENDF/B-VIII.0			
	k_{eff}	1σ unc	k_{calc}	95% CI	EALF (MeV)	C/E-1
1	0.99953	0.00195	1.00956	0.00022	$1.0259 \cdot 10^{-1}$	0.01003
2	0.99938	0.00154	1.00771	0.00022	$1.6386 \cdot 10^{-2}$	0.00834
3	1.00008	0.00154	1.00720	0.00022	$8.5769 \cdot 10^{-4}$	0.00712
4	1.00078	0.00142	1.00272	0.00024	$3.3099 \cdot 10^{-5}$	0.00194
5	0.99871	0.00121	0.99952	0.00024	$2.9528 \cdot 10^{-6}$	0.00081
			JENDL-5.0			
1	0.99953	0.00195	1.01063	0.00020	$9.50 \cdot 10^{-2}$	0.01111
2	0.99938	0.00154	1.01333	0.00020	$1.51 \cdot 10^{-2}$	0.01396
3	1.00008	0.00154	1.01458	0.00020	$8.07 \cdot 10^{-4}$	0.01450
4	1.00078	0.00142	1.01020	0.00022	$3.20 \cdot 10^{-5}$	0.00941
5	0.99871	0.00121	1.00561	0.00024	$2.89 \cdot 10^{-6}$	0.00691
			JEFF-3.3			
1	0.99953	0.00195	1.01639	0.00022	$1.0302 \cdot 10^{-1}$	0.01687
2	0.99938	0.00154	1.01632	0.00020	$1.6126 \cdot 10^{-2}$	0.01695
3	1.00008	0.00154	1.01493	0.00022	$8.4136 \cdot 10^{-4}$	0.01485
4	1.00078	0.00142	1.00891	0.00024	$3.2526 \cdot 10^{-5}$	0.00812
5	0.99871	0.00121	1.00423	0.00024	$2.9241 \cdot 10^{-6}$	0.00553
			Present work			
1	0.99953	0.00195	1.01032	0.00022	$1.022 \cdot 10^{-1}$	0.01069
2	0.99938	0.00154	1.00709	0.00022	$1.640 \cdot 10^{-2}$	0.00732
3	1.00008	0.00154	1.00479	0.00024	$8.664 \cdot 10^{-4}$	0.00460
4	1.00078	0.00142	1.00141	0.00024	$3.324 \cdot 10^{-5}$	0.00041
5	0.99871	0.00121	0.99955	0.00022	$2.948 \cdot 10^{-6}$	0.00067

Results for PMM003, cases 1–5, are provided in Table 4, which shows the published benchmark k_{eff} with uncertainty (1σ), the MCNP calculated k_{calc} with uncertainty (95% CI), the energy corresponding to the average neutron lethargy causing fission (EALF), and the value $C/E-1$, where C represents the MCNP calculated k_{calc}, and E represents the published benchmark k_{eff}.

The data are plotted in Fig. 11, showing the trends in $C/E-1$ as a function of EALF, and they are consistent with results obtained in Ref. Barry et al. (2024), with a similar increasing bias in $C/E-1$ with increasing neutron spectrum hardness. Relative to the RRR modifications (Barry et al., 2024) alone, incorporating the URR modifications from the present work was observed to have little impact on $C/E-1$ values for cases 3–5, and the modification increased them slightly for cases 1–2, as shown in Fig. 12. This is due to a reduction in ^{181}Ta absorptions in the URR for these cases, as shown in Fig. 13, and a corresponding increase in k_{calc}.

It should also be noted that nuclear data uncertainties were not included in the transport models shown above. Nuclear data uncertainty is a significant contributor to the total uncertainty in the majority of radiation transport models. To demonstrate that impact, values for k_{calc} using TSUNAMI (Wieselquist and Lefebvre, 2021) are given in Fig. 14. The uncertainties are taken from the SCALE ENDF/B-VIII.0 covariance library (Wieselquist and Lefebvre, 2021), except for the ^{181}Ta, which used covariances from the resolved and unresolved evaluations described here. The most significant contributor to total uncertainty on k_{calc} was ^{239}Pu(n,f) for cases 1–3, and ^{239}Pu(n, γ) for cases 4–5. The first and second most significant contributors to total uncertainty from the ^{181}Ta evaluation for cases 2–5 was ^{181}Ta(n, γ) and ^{181}Ta(n,n'), and for case 1 it was ^{181}Ta(n,n) and ^{181}Ta(n, γ).

Based on results for this particular benchmark, the evaluation proposed in this work represents an improvement over the ENDF/B-VIII.0 ^{181}Ta evaluation. However, the high C/E values for cases 1–3 suggest that there is still much room for improvement. Given the neutron spectra associated with these cases, it is likely that improvements in the fast range cross sections will improve criticality results. The finalized ENDF/B library is expected to address the issues in high energy cross sections of ^{181}Ta.

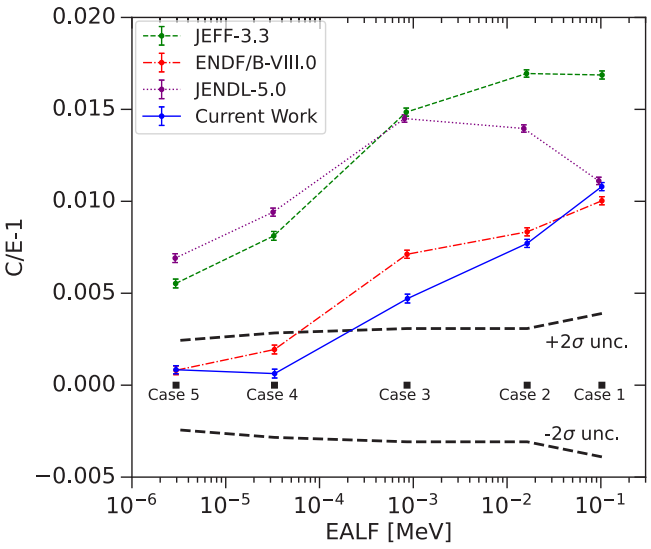

Fig. 11. Validation results for PMM003 showing increasing reactivity trends with increasing neutron spectrum hardness, for ENDF/B-VIII.0, JEFF 3.3, JENDL 5.0, and the present work.

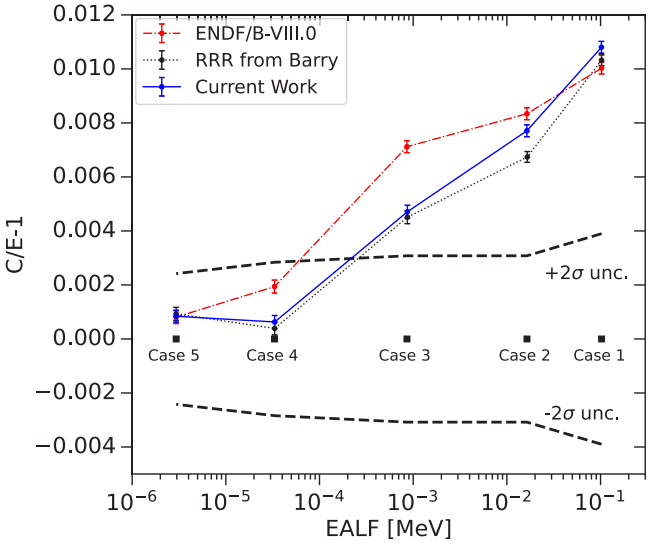

Fig. 12. Comparison of PMM003 results using unmodified ^{181}Ta from ENDF/B-VIII.0, RRR modifications from Barry et al. (2024), and URR modifications from the present work.

5. Conclusion

In this work, the URR for ^{181}Ta was re-evaluated based on recent measurements by Brown et al. (2023) and other measurements from EXFOR that included uncertainty information and sufficient documentation. Updated average parameters in the current evaluation improve modeling for thick-sample neutron transmission and capture rate, as demonstrated by comparison to the energy-differential thick-sample transmission and self-shielding measurements by Byoun (1973a,b) and Brown et al. (2020). Applying those same cross sections to criticality models, on the other hand, caused the modeled k_{calc} to deviate from the measured value slightly more than ENDF/B-VIII.0. This deviation seems to be due to the reduced capture cross section in the URR—the very same change that improved agreement with differential measurements. This leads the authors to believe that cross section changes in other materials in the PMM003 benchmark may be necessary to improve agreement with the measured values, in addition to the changes in

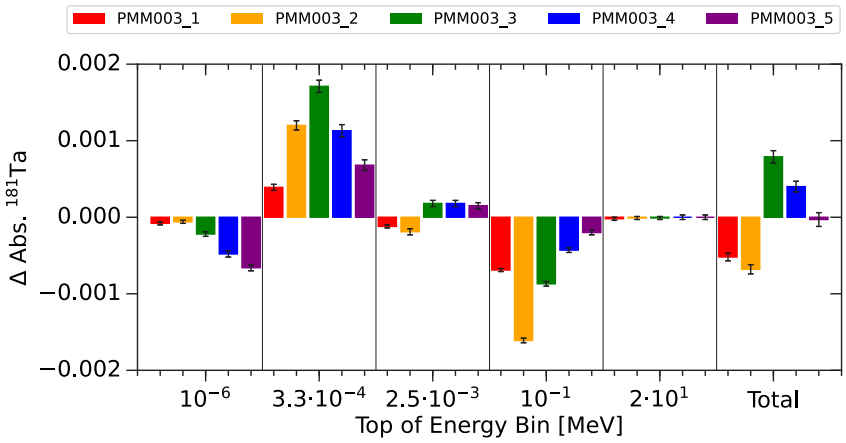

Fig. 13. Differences in PMM003 ^{181}Ta absorption rates over various energy ranges (Present Work–ENDF/B-VIII.0). The URR spans the energy range of 2.5–100 keV. Note the decrease in ^{181}Ta absorption rates over the URR and the corresponding impact to total ^{181}Ta absorptions in the model.

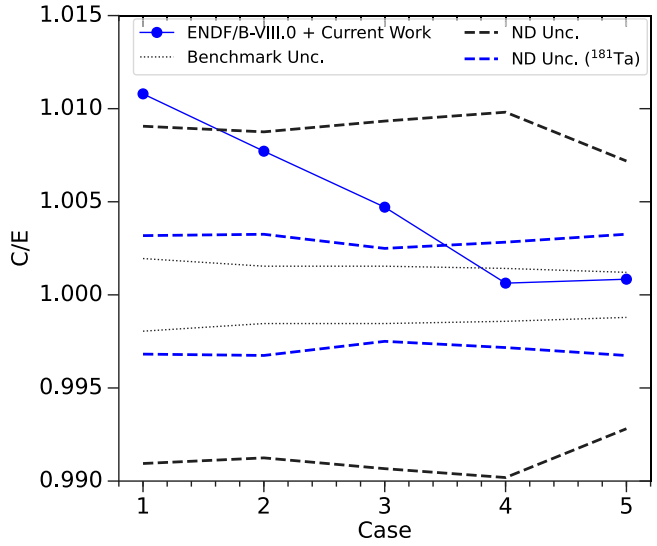

Fig. 14. Nuclear data uncertainty from the SCALE ENDF/B-VIII.0 library was modified to include the current work's covariances in the RRR and URR (including Barry et al. (2024)) and propagated to nuclear data uncertainty in the PMM003 benchmark. In the figure, "Benchmark Unc". is the experimental uncertainty and "ND Unc". is the propagated error from cross section uncertainties and "ND Unc. (^{181}Ta)" is the propagated uncertainty from only the new RRR and URR evaluations.

high-energy cross sections of ^{181}Ta expected in the ENDF/B-VIII.1 library.

Declaration of competing interest

The authors declare the following financial interests/personal relationships which may be considered as potential competing interests: Jesse M Brown reports financial support was provided by National Nuclear Security Administration. If there are other authors, they declare that they have no known competing financial interests or personal relationships that could have appeared to influence the work reported in this paper.

Acknowledgments

This work was supported by the Nuclear Criticality Safety Program, funded and managed by the National Nuclear Security Administration for the Department of Energy. ORNL is managed by UT-Battelle, LLC, under Contract No. DE-AC05-00OR22725 for the U.S. Department of Energy.

Table A.5
Labels CAP, TOT, and ELA represent neutron capture cross section, total cross section, and elastic cross section respectively. Different datasets from Brown et al. (2023) are differentiated by sample thickness, different datasets from Wisshak et al. (1990, 2004) are differentiated by year. Prior normalization uncertainties include multiple sources of experimental systematic uncertainty, including unrecognized sources of uncertainty. Posterior normalizations are used to compare experimental cross section to normalized theoretical cross section calculated by SAMMY.

Dataset	Type	Prior	Posterior
Brown 1 mm	CAP	1.0 ± 0.08	0.961 ± 0.016
Brown 2 mm	CAP	1.0 ± 0.08	0.977 ± 0.015
Brown 1 mm	TOT	1.0 ± 0.05	1.008 ± 0.028
Brown 3 mm	TOT	1.0 ± 0.05	0.987 ± 0.014
Brown 6 mm	TOT	1.0 ± 0.05	0.966 ± 0.011
Wisshak '90	CAP	1.0 ± 0.02	0.985 ± 0.014
Wisshak '04	CAP	1.0 ± 0.04	0.986 ± 0.016
Brzosko	CAP	1.0 ± 0.08	1.095 ± 0.022
Shorin	CAP	1.0 ± 0.08	0.987 ± 0.021
Yamamuro	CAP	1.0 ± 0.08	0.940 ± 0.020
Kononov	CAP	1.0 ± 0.08	1.084 ± 0.019
Bokhovko	CAP	1.0 ± 0.08	0.909 ± 0.016
McDermott	CAP	1.0 ± 0.08	1.015 ± 0.020
Vertebnyy	TOT	1.0 ± 0.05	1.005 ± 0.012
Poenitz.	TOT	1.0 ± 0.01	0.992 ± 0.009
Zo	ELA	1.0 ± 0.10	0.963 ± 0.014

Appendix. Experimental parameter adjustment

The normalization factors, n, used in the SAMMY fit where normalized theoretical cross sections are given by $n \cdot \sigma_{*,theory}$ and the corresponding normalization uncertainties are given in Table A.5. These normalization uncertainties represent uncertainty from multiple experimental contributions and unrecognized sources of uncertainty. Posterior values are calculated from the Bayesian analysis with SAMMY, and only applied for the comparison with the data to evaluate the average resonance parameters. The final cross sections reported come straight from the final posterior parameters without any normalization. CAP, TOT, and ELA represent neutron capture cross section, total cross section, and elastic cross section respectively.

Data availability

Data will be made available on request.

References

Barry, D., Lewis, A., Leal, L., Brown, J., 2023. A new ^{103}Rh Unresolved Resonance Region evaluation. Ann. Nucl. Energy 188, 109751. http://dx.doi.org/10.

1016/j.anucene.2023.109751, URL https://www.sciencedirect.com/science/article/pii/S0306454923000701.

Barry, D.P., Pigni, M.T., Brown, J.M., Lewis, A.M., Trumbull, T.M., Guber, K.H., McDermott, B.J., Block, R.C., Danon, Y., 2024. A new ^{181}Ta neutron Resolved Resonance Region evaluation. Ann. Nucl. Energy (ISSN: 0306-4549) 208, 110778. http://dx.doi.org/10.1016/j.anucene.2024.110778, https://www.sciencedirect.com/science/article/pii/S0306454924004419.

Bokhovko, M., Voevodskij, A., Kononov, V., Poletaev, E., Timokhov, V., 1991. Cross Sections of Fast Neutron Capture and Transmission for the Rare Earth Element Isotopes, ^{181}Ta, and ^{187}Os. Tech. Rep. FEI–2169, Gosudarstvennyj Komitet po Ispol'zovaniyu Atomnoj Ehnergii SSSR.

Brown, J.M., 2019. Measurements, Evaluation, and Validation of Ta-181 Resolved and Unresolved Resonance Regions (Ph.D. dissertation). Dept. Mech. Aero. and Nuc. Eng., Rensselaer Polytechnic Inst., Troy, NY.

Brown, J.M., Barry, D.P., Block, R.C., Youmans, A., Choun, H., Ney, A., Blain, E., Rapp, M.J., Danon, Y., 2023. New measurements to resolve discrepancies in evaluated model parameters of ^{181}Ta. Nucl. Sci. Eng. 198 (6), 1155–1165. http://dx.doi.org/10.1080/00295639.2023.2249786.

Brown, J.M., Block, R., Youmans, A., Choun, H., Ney, A., Blain, E., Barry, D., Rapp, M., Danon, Y., 2020. Validation of unresolved neutron resonance parameters using a thick-sample transmission measurement. Nucl. Sci. Eng. 194 (3), 221–231.

Brown, D., et al., 2018. ENDF/B-VIII.0: The 8th major release of the nuclear reaction data library with CIELO-project cross sections, new standards and thermal scattering data. Nucl. Data Sheets 148, 1–142. http://dx.doi.org/10.1016/j.nds.2018.02.001, URL http://www.sciencedirect.com/science/article/pii/S0090375218300206. (Accessed 2 July 2019).

Brzosko, J., Gierlik, E., Soltan, Jr., A., Wilhelmi, Z., 1969. Effect of the pigmy resonance on the calculations of the neutron capture cross section. Can. J. Phys. 47 (24), 2849–2857.

Byoun, T.Y., 1973a. Experimental Investigation of the Resonance Self-Shielding and Doppler Effect in Uranium and Tantalum. Tech. Rep. 3058-34, Chicago Operations Office, AEC, Chicago, Illinois, USA.

Byoun, T.Y., 1973b. Experimental Investigation of the Resonance Self-Shielding and Doppler Broadening Effect in Uranium and Tantalum (Doctoral Thesis). Rensselaer Polytechnic Institute, Troy, NY.

Carlson, A.D., Pronyaev, V.G., Capote, R., Hale, G.M., Chen, Z.-P., Duran, I., Hambsch, F.-J., Kunieda, S., Mannhart, W., Marcinkevicius, B., et al., 2018. Evaluation of the neutron data standards. Nucl. Data Sheets 148, 143–188.

Carlson, A., et al., 2009. International evaluation of neutron cross section standards. Nucl. Data Sheets 110 (12), 3215–3324.

Conlin, J.L., Haeck, W., Neudecker, D., Parsons, D.K., White, M.C., 2018. Release of ENDF/B-VIII.0-Based ACE Data Files. Tech. Rep. LA-UR-18-24034, Los Alamos National Laboratory, Los Alamos, NM, USA,.

El-Dasher, B., Farmer, J., Ferreira, J., de Caro, M.S., Rubenchik, A., Kimura, A., 2011. Corrosion of oxide dispersion strengthened iron–chromium steels and tantalum in fluoride salt coolant: An in situ compatibility study for fusion and fusion–fission hybrid reactor concepts. J. Inst. Nucl. Mater. Manage. 419 (1–3), 15–23.

Fritz, D., 2022. Design of a Cold Moderator for Total Cross Section Measurements of Moderator Materials at Sub-Thermal Energies (Ph.D. thesis). Rensselaer Polytechnic Institute.

Fröhner, F., 1968. SESH - A FORTRAN IV Code for Calculating the Self-Shielding and Multiple Scattering Effects for Neutron Cross Section Data Interpretation in the Unresolved Resonance Region. Tech. Rep. GA-8380, Gulf General Atomic, Inc., San Diego, CA, USA.

Fröhner, F., Brown, J.M., 2021. Sesh, [computer software]. http://dx.doi.org/10.11578/dc.20211001.4.

Gilbert, A., Cameron, A.G.W., 1965. A composite nuclear-level density formula with shell corrections. Can. J. Phys. 43 (8), 1446–1496. http://dx.doi.org/10.1139/p65-139.

Harvey, J., Hill, N., Perey, F., Tweed, G., Leal, L., 1988. High-Resolution Neutron Transmission Measurements on ^{235}U, ^{239}Pu, and ^{238}U. Tech. Rep. CONF-880546, ORNL, Oak Ridge, TN, USA.

Herman, M., Kawano, T., 2024. Private communication.

2022. International Handbook of Evaluated Criticality Safety Benchmark Experiments. Tech. Rep., Organisation for Economic Cooperation and Development Nuclear Energy Agency, Paris, France.

Iwamoto, O., et al., 2019. Status of JENDL. In: ND 2019: International Conference on Nuclear Data for Science and Technology, Beijing, China, May 12-16.

Kirkbride, L., 1965. Molten Plutonium Alloys as Fast Reactor Fuels. Tech. Rep. LA-DC-7336, LANL, Los Alamos, NM, USA.

Koning, A., Rochman, D., Sublet, J.-C., Dzysiuk, N., Fleming, M., van der Marck, S., 2019. TENDL: Complete nuclear data library for innovative nuclear science and technology. Nucl. Data Sheets 155, 1–55. http://dx.doi.org/10.1016/j.nds.2019.01.002, URL https://www.sciencedirect.com/science/article/pii/S009037521930002X. Special Issue on Nuclear Reaction Data.

Kononov, V., Jurlov, B., Manturov, G., Poletaev, E., Timokhov, V., Shorin, V., 1977. Fast neutron radiative capture cross-section for In-115, Ta-181, Au-197 and samarium and europium isotopes. Sov. J. Nucl. Phys. 26, 500.

Lane, A.M., Thomas, R.G., 1958. R-matrix theory of nuclear reactions. Rev. Modern Phys. 30 (2), 257–353. http://dx.doi.org/10.1103/RevModPhys.30.257.

Larson, N., 2008. Updated Users' Guide For SAMMY: Multilevel R-Matrix Fits to Neutron Data Using Bayes' Equations. Tech. Rep. ORNL/TM-9179/R8, ORNL, Oak Ridge, TN, USA.

Leal, L., et al., 2011. Assessment of the Unresolved Resonance Treatment for Cross-section and Covariance Representation. Tech. Rep. NEA/WPEC-32, Organisation for Economic Cooperation and Development, Nuclear Energy Agency.

MacFarlane, R., Muir, D.W., Boicourt, R.M., Kahler, III, A.C., Conlin, J.L., 2017. The NJOY Nuclear Data Processing System, Version 2016. Tech. Rep. LA-UR-17-20093, LANL, Los Alamos, NM, USA, http://dx.doi.org/10.2172/1338791.

Malter, L., Langmuir, D., 1939. Resistance, emissivities and melting point of tantalum. Phys. Rev. 55 (8), 743–747.

McDermott, B., 2016. Resonance Region Capture Cross Section Measurements in Iron and Tantalum Using a New C6D6 Detector Array (Ph.D. dissertation). Dept. Mech. Aero. and Nuc. Eng., Rensselaer Polytechnic Inst., Troy, NY.

McDermott, B.J., et al., 2017. ^{181}Ta(n,γ) cross section and average resonance parameter measurements in the unresolved resonance region from 24 to 1180 keV using a filtered-beam technique. Phys. Rev. C 96 (1), 014607. http://dx.doi.org/10.1103/PhysRevC.96.014607, URL https://link.aps.org/doi/10.1103/PhysRevC.96.014607.

Members of the CSWEG, 2018. ENDF-6 Formats Manual. Tech. Rep. BNL-203218-2018-INRE, BNL, Upton, NY, USA.

Mughabghab, S., 2006. Atlas of Neutron Resonances, fifth ed. Elsevier, Amsterdam, The Netherlands.

Mughabghab, S., 2018. Atlas of Neutron Resonances, sixth ed. Vol. 2, Elsevier, Amsterdam, The Netherlands.

Mullins, L., Beaumont, A., Leary, J., 1968. Distribution of americium between liquid plutonium and a fused salt. Evidence for divalent americium. J. Inorg. Nucl. Chem. 30 (1), 147–156.

Otuka, N., et al., 2014. Towards a more complete and accurate experimental nuclear reaction data library (EXFOR): International collaboration between nuclear reaction data centres (NRDC). Nucl. Data Sheets 120 (1), 272–276. http://dx.doi.org/10.1016/j.nds.2014.07.065.

Overberg, M., Moretti, B., Slovacek, R., Block, R., 1999. Photoneutron target development for the RPI linear accelerator. Nucl. Instrum. Methods Phys. Res. A 438 (2), 253–264. http://dx.doi.org/10.1016/S0168-9002(99)00878-5, URL http://www.sciencedirect.com/science/article/pii/S0168900299008785. (Accessed 3 July 2019).

Percher, C., Bess, J., Marshall, W., Martin, J.-F., Hill, I., Ivanova, T., 2023. Status of the international criticality safety benchmark evaluation project. In: ICNC 2023 - The 12th International Conference on Nuclear Criticality Safety October 1st – 6th, 2023 in Sendai, Japan.

Plompen, A.J., Cabellos, O., De Saint Jean, C., Fleming, M., Algora, A., Angelone, M., Archier, P., Bauge, E., Bersillon, O., Blokhin, A., et al., 2020. The joint evaluated fission and fusion nuclear data library, JEFF-3.3. Eur. Phys. J. A 56, 1–108.

Poenitz, W., Whalen, J., Smith, A., 1981. Total neutron cross sections of heavy nuclei. Nucl. Sci. Eng. 78 (4), 333–341.

Roy, J., et al., 1996. Thermodynamic properties of U, Np, Pu, and Am in molten LiCl-KCl eutectic and liquid cadmium. J. Electrochem. Soc. 143 (8), 2487–2492.

Taylor, D.F., 1950. Acid corrosion resistance of Tantalum, Columbium, Zirconium, and Titanium. Ind. Eng. Chem. 42 (4), 639.

Werner, C.J., Armstrong, J.C., Brown, F.B., Bull, J.S., Casswell, L., Cox, L.J., Dixon, D.A., Forster, III, R.A., Goorley, J.T., Hughes, III, H.G., Favorite, J.A., Martz, R.L., Mashnik, S.G., Rising, M.E., Solomon, Jr., C.J., Sood, A., Sweezy, J.E., Zukaitis, A.J., Anderson, C.A., Elson, J.S., Durkee, Jr., J.W., Johns, R.C., McKinney, G.W., McMath, G.E., Hendricks, J.S., Pelowitz, D.B., Prael, R.E., Booth, T.E., James, M.R., Fensin, M.L., Wilcox, T.A., Kiedrowski, B.C., 2017. MCNP User's Manual Code Version 6.2. Tech. Rep. LA-UR-17-29981, Los Alamos National Laboratory, Los Alamos, NM, USA, URL http://permalink.lanl.gov/object/tr?what=info:lanl-repo/lareport/LA-UR-17-29981.

Wieselquist, W.A., Lefebvre, R.A., 2021. SCALE 6.3.0 User Manual. Tech. Rep. ORNL/TM-SCALE-6.3.0, ORNL, Oak Ridge, TN, USA.

Wisshak, K., Voss, F., Arlandini, C., Käppeler, F., Heil, M., Reifarth, R., Krtička, M., Bečvář, F., 2004. Stellar neutron capture on ^{180}Ta^{m}. I. Cross section measurement between 10 keV and 100 keV. Phys. Rev. C 69 (5), 055801.

Wisshak, K., Voss, F., Käppeler, F., Reffo, G., 1990. Measurements of keV neutron capture cross sections with a 4π barium fluoride detector: Examples of ^{93}Nb, ^{103}Rh, and ^{181}Ta. Phys. Rev. C 42 (4), 1731–1750. http://dx.doi.org/10.1103/PhysRevC.42.1731, URL https://link.aps.org/doi/10.1103/PhysRevC.42.1731.

Wu, S.-C., 2005. Nuclear data sheets for A=181. Nucl. Data Sheets 106 (3), 367–600. http://dx.doi.org/10.1016/j.nds.2005.11.001, URL https://www.sciencedirect.com/science/article/pii/S0090375205000840.

Yamamuro, N., Saito, K., Emoto, T., Wadam, T., Fujita, Y., Kobayashi, K., 1980. Neutron capture cross section measurements of Nb-93, I-127, Ho-165, Ta-181, and U-238 between 3.2 and 80 keV. J. Nucl. Sci. Technol. 17 (8), 582–592.

Zo, I.O., Nikolenko, V., Popov, A., Samosvat, G., 1985. The Neutron Elastic Scattering Differential Cross Sections in Energy Range Below 440 kev. Tech. Rep., Joint Inst. for Nuclear Research.